ISSN 1674-1056
http://cpb.iphy.ac.cn
http://iopscience.iop.org/cpb
中国物理 B
Chinese Physics
中国物理
Chinese Physics B

Optoelectronic memristor for neuromorphic computing

Wuhong Xue(薛武红), Wenjuan Ci(次文娟), Xiao-Hong Xu(许小红), Gang Liu(刘钢)

Citation: Chin. Phys. B . 2020, 29(4): 048401 . **doi:** 10.1088/1674-1056/ab75da
Journal homepage: http://cpb.iphy.ac.cn; http://iopscience.iop.org/cpb

What follows is a list of articles you may be interested in

Exponential flux-controlled memristor model and its floating emulator

Liu Wei, Wang Fa-Qiang, Ma Xi-Kui

Chin. Phys. B . 2015, 24(11): 118401 . **doi:** 10.1088/1674-1056/24/11/118401

Switching mechanism for TiO_2 memristor and quantitative analysis of exponential model parameters

Wang Xiao-Ping, Chen Min, Shen Yi

Chin. Phys. B . 2015, 24(8): 088401 . **doi:** 10.1088/1674-1056/24/8/088401

Toward the complete relational graph of fundamental circuit elements

Shang Da-Shan, Chai Yi-Sheng, Cao Ze-Xian, Lu Jun, Sun Young

Chin. Phys. B . 2015, 24(6): 068402 . **doi:** 10.1088/1674-1056/24/6/068402

Threshold flux-controlled memristor model and its equivalent circuit implementation

Wu Hua-Gan, Bao Bo-Cheng, Chen Mo

Chin. Phys. B . 2014, 23(11): 118401 . **doi:** 10.1088/1674-1056/23/11/118401

Memristance controlling approach based on modification of linear *M-q* curve

Liu Hai-Jun, Li Zhi-Wei, Yu Hong-Qi, Sun Zhao-Lin, Nie Hong-Shan

Chin. Phys. B . 2014, 23(11): 118402 . **doi:** 10.1088/1674-1056/23/11/118402

TOPICAL REVIEW — Physics in neuromorphic devices

Optoelectronic memristor for neuromorphic computing*

Wuhong Xue(薛武红)[1,2,†], Wenjuan Ci(次文娟)[1,†], Xiao-Hong Xu(许小红)[1,‡], and Gang Liu(刘钢)[2,3,§]

[1] *Key Laboratory of Magnetic Molecules and Magnetic Information Materials of Ministry of Education, School of Chemistry and Materials Science, Shanxi Normal University, Linfen* 041004, *China*
[2] *School of Chemistry and Chemical Engineering, Shanghai Jiao Tong University, Shanghai* 200240, *China*
[3] *College of Chemistry and Molecular Engineering, Zhengzhou University, Zhengzhou* 450001, *China*

(Received 8 January 2020; revised manuscript received 5 February 2020; accepted manuscript online 13 February 2020)

With the need of the internet of things, big data, and artificial intelligence, creating new computing architecture is greatly desired for handling data-intensive tasks. Human brain can simultaneously process and store information, which would reduce the power consumption while improve the efficiency of computing. Therefore, the development of brain-like intelligent device and the construction of brain-like computation are important breakthroughs in the field of artificial intelligence. Memristor, as the fourth fundamental circuit element, is an ideal synaptic simulator due to its integration of storage and processing characteristics, and very similar activities and the working mechanism to synapses among neurons which are the most numerous components of the brains. In particular, memristive synaptic devices with optoelectronic responding capability have the benefits of storing and processing transmitted optical signals with wide bandwidth, ultrafast data operation speed, low power consumption, and low cross-talk, which is important for building efficient brain-like computing networks. Herein, we review recent progresses in optoelectronic memristor for neuromorphic computing, including the optoelectronic memristive materials, working principles, applications, as well as the current challenges and the future development of the optoelectronic memristor.

Keywords: memristor, optoelectronic, neuromorphic computing

PACS: 84.37.+q, 87.19.lw, 87.19.lv, 84.35.+i **DOI:** 10.1088/1674-1056/ab75da

1. Introduction

In recent years, as the information technology advances increasingly faster, the economical-technical Moore's law that well dominated the past-century evolution of the semiconductor and integrated circuit industry is about to reach its limits in the foreseeable future at about the 2–3 nm node.[1] Simultaneously, due to the limitations of the traditional von Neumann computer architecture that generate significant latency and power consumption during frequent data movement between the physically separated central processing unit (CPU) and the memory hierarchy,[2,3] the pace of the overall computing performance improvement gradually slows down. New computing paradigms are greatly desired to repower the capability that human society deals with the big data. Mammalian brain has the ability to simultaneously store, integrate, and process information through a densely coordinated network of synapses and neurons,[4] which can greatly reduce the power consumption and improve the data management efficiency in the meanwhile when handling the analog signals detected by the sensory organs (e.g., visual information received by the retina). Inspired by the human brain's high integration of information processing and storage, neuromorphic computing utilizing artificial neural networks built from man-made neurons and synapses is expected to break through the von Neumann bottleneck to achieve efficient and low-cost information manipulation.

Since the conceptual propose by Chua in 1971[5] and its first device demonstration in 2008,[6] memristor, as the fourth basic electronic circuit element in addition to the long-established resistor, capacitor, and inductor, is a two-terminal resistor built from top and bottom electrodes and intermediate insulating dielectric layer, and carries memory function that memorizes the new resistance state induced by voltage and current. Generally, the conductance states of a memristor can be modulated non-volatilely and reversibly through an external electric field, including steep (digital) and gradual (analog) changes in conductance.[7] The former can be used for storing and processing information, and the latter is used to simulate synaptic due to similarity to biological synapses in both the device architecture and the electrical behaviors (Figs. 1(a) and 1(b)). The electric set process corresponds to the transition from the low conductance state to high conductance state. The electric reset process is switching the device back to the low conductance state. Among them, the gradual conductance

*Project supported by the National Key R&D Program of China (Grant No. 2017YFB0405600), the National Natural Science Foundation of China (Grant Nos. 61674153, 61722407, 61974090, and 61904099), and the Natural Science Foundation of Shanghai, China (Grant No. 19ZR1474500).

†These authors contributed equally to this work.
‡Corresponding author. E-mail: xuxh@sxnu.edu.cn
§Corresponding author. E-mail: gang.liu@sjtu.edu.cn

© 2020 Chinese Physical Society and IOP Publishing Ltd

change by voltage and current in the memristor resembles the updating of synaptic weights in biological neural systems and thus makes possible the emulation of basic synapse functions including short-term plasticity (STP), long-term potentiation (LTP), long-term depression (LTD), and spike timing dependent plasticity (STDP).[8,9] The physical mechanism of this transformation is currently explained by the conductive filament (CF) model (Fig. 1(c))[10,11] and the barrier variation model (Fig. 1(d)).[12] In the CF mode, the electric field triggers the migration and redistribution of active electrode metallic cations/oxygen anions existing in the switching materials to form and break CFs in the switching layers. In the barrier variation model, the energy band diagram of the switching matrix sandwiched between two electrodes can be modified by the applied bias. The two-terminal structure, as well as the inherent multiply-accumulate (MAC) capability through the Ohm's law and Kirchhoff's law, also allows the construction of crossbar array artificial neural network for object and speech recognition, autonomous vehicles, robotics, medicine and finance applications, etc (Fig. 1(e)).[13]

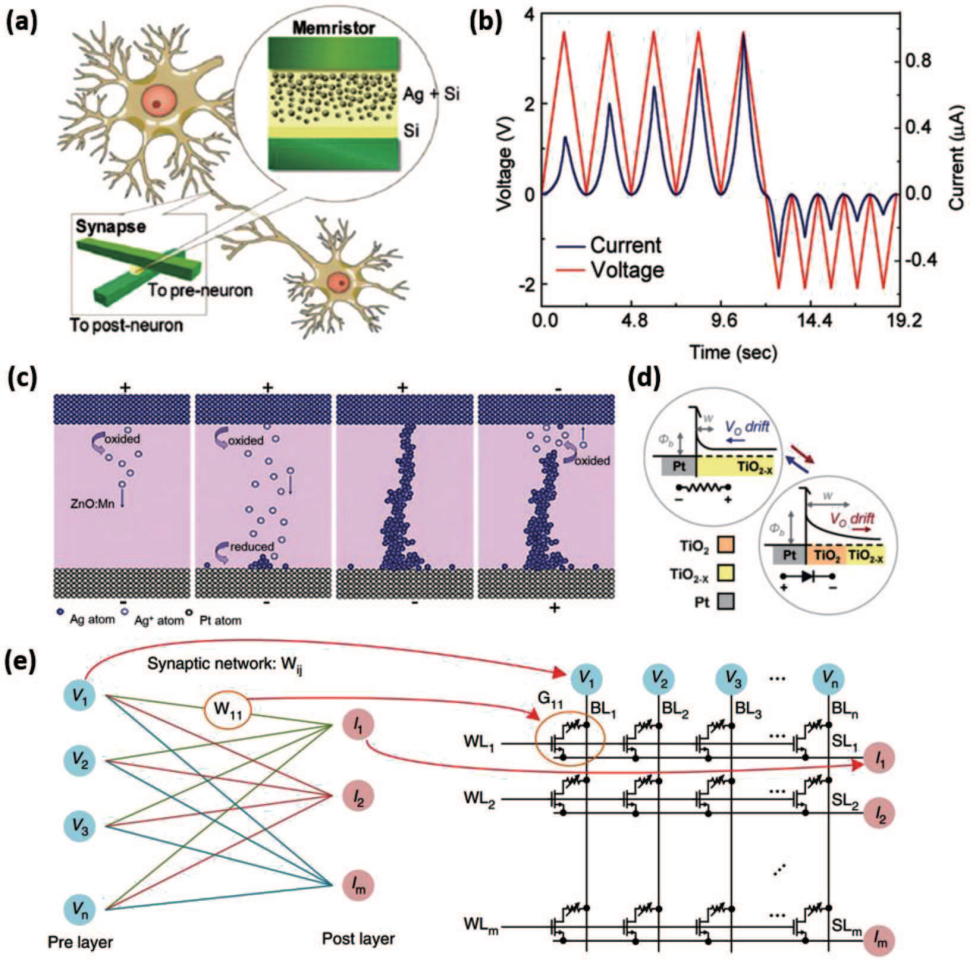


Fig. 1. (a) Schematic illustration of memristors used as synapses connecting pre-neuron and post-neuron and (b) the change of current in repeated voltage sweeps.[8] Copyright (2010) American Chemical Society. Schematic drawings of resistive switching modes with (c) formation and rupture of a filament[10] and (d) modification of the Schottky barrier height[12] through voltage driving ion migration. Copyright (2009) American Chemical Society and Copyright (2009) John Wiley & Sons, Inc. (e) Mapping of a neural network on the one transistor and one memristor array.[13] Copyright (2017) Springer Nature.

Excitingly, when light regulation is introduced in memristors as an additional dimension of control approach to regulate the evolution of the CFs or the interfacial barriers, the device conductance can be modified by both pure optical means with different wavelength and intensity of the illumination, and the synergistic interplay between the optical and electric fields. Benefiting from the ultrafast operation speed, virtually unlimited bandwidth, avoidance of the crosstalk interference, elimination of electrical Joule heating, and the potential of functional integration involving optical signal sensing, handling, and storing in a single cell, optoelectronic memristors are considered as promising candidates for multifunctional neuromorphic computing (artificial visual systems, in particular) applications.[14,15]

In this contribution, we are aiming to give a timely and comprehensive review of the recent progress on the optoelectronic memristor that covers all the material, mechanism, device aspects, and briefly discuss their potential application sce-

nario and future developments. Focus will be first concentrated on the photosensitive material systems that can be employed in optoelectronic memristive switching effects, classifying as inorganic metal oxides, organics, organic–inorganic halide perovskites, and two-dimensional (2D) materials. Afterwards, the working principles of optoelectronic memristor devices, including the light-induced or light-assisted modulation of the interface barrier, molecular isomerization, ion diffusion, chemical reaction, and structural transition, are discussed. Finally, a brief overview of the device application in neuromorphic computing, some important challenges, and future prospective research areas is summarized.

2. Materials systems for optoelectronic memristor

To physically implement optoelectronic memristors, photosensitive semiconductor or insulating materials should be used as the switching matrix. Till date, various of materials, including the metal oxide system, organic materials, organic–metal halide perovskite, and 2D materials, have been proposed to be used in constructing optoelectronic memristive devices.[16]

2.1. Metal oxide systems

Metal oxides, having excellent optical, electrical, and magnetic properties, are important fundamental materials in the fields of electronic and energy devices.[17–19] In particular, the oxygen defect contents of oxide semiconductors can be regulated efficiently by external fields, which allows the easy modulation of their Fermi energy level and conductance for optoelectronic applications.[20,21] At present, binary, ternary, and complex metal oxides are widely used in optoelectronic memristors.

Due to the fluorite geometry that can tolerate the presence of oxygen vacancy defects inside the lattice while maintain its crystalline structure complete, binary cerium oxide (CeO_2) is widely explored as an active material in electrocatalysis (e.g., oxygen reduction reactions, ORR) areas. More importantly, the introduction of the defect energy levels into the bandgap of the material also leads to a good optical response in the broad spectrum from ultraviolet (UV) to visible range.[22–25] Therefore, using CeO_2 as the photosensitive dielectric layer in memristor devices may result in possible optoelectronic modulation characteristics.[17,18] Tan *et al.* designed an optoelectronic memristor with cerium oxide as the switching layer, and transparent conductive oxide indium-tin oxide (ITO) and aluminum (Al) as the top/bottom electrodes, respectively (Fig. 2(a)).[17,18] A natively oxidized aluminum oxide layer (AlO_y) is expected to exist as an intercalation layer at the oxide/Al interface, constituting the device structure of ITO/CeO_{2-x}/AlO_y/Al. The charge carriers trapped by the oxygen vacancies at the CeO_{2-x}/AlO_y/Al interfacial region may be excited by optical illumination, extracted by external electric field and redistributed from the interface, which in turn modulates the Schottky barrier width and device resistance with persistent photoconductivity characteristics. When a positive voltage is applied to the ITO electrode, oxygen vacancies are driven by the electric field across the cerium oxide layer towards the Al cathode and get accumulated at the CeO_{2-x}/AlO_y/Al interface, a slight hysteresis can be observed in the current–voltage (I–V) curve of the device. Upon being exposed to white light illumination with the optical power of 60 pW/μm^2 for 20 s, the device can be programmed from the initial high resistance state (HRS) into a lower resistance ($\sim 1\times10^9$ Ω) state (LRS) with the ON/OFF ratio of ~ 30. The low resistance state can be well maintained after removing the optical stimuli, indicating that the observed photoresponse in the ITO/CeO_{2-x}/AlO_y/Al device has a persistent nature and is applicable to nonvolatile data storage applications.

Different from what happens in cerium oxide, the light-induced manipulation of molybdenum valence states in the molybdenum oxide thin film may also give rise to device resistance changes.[26–28] Zhou and co-workers designed a Pb/MoO_x/ITO optoelectronic memristor for storing the optical information and executing light-tunable synaptic functions.[26] Cai *et al.*[27] designed and constructed a hybrid Au/PMMA/Ag/MoO_3/P_3HT:PCBM/ZnO/ITO device (inset of Fig. 2(b)) to store and manipulate optical and electronic information. ZnO, P_3HT:PCBM, and MoO_3 were used as the electron transport layer, the photosensitive layer, and the hole transport layer, respectively. Besides electric field, light can also induce a nonvolatile transition from low current to high current (Fig. 2(b)). Doping of wide bandgap oxide semiconductor can also lead to photo response to the visible light. Akbari *et al.* fabricated a Pt/In-doped TiO_2/Au memristor device, in which the indium cation migration and oxygen vacancy movement co-exist.[29] When the device is irradiated by the visible light, the voltage required to convert it to a low-resistance state becomes significantly smaller, indicating that the HRS–LRS transition is much easier under optical stimulation. As the light intensity increases, the switching voltages decrease continuously. Ingeniously, Zhao *et al.*[30] utilized the TiO_2 photocatalytic reduction to locally generate reduced graphene oxide domains in the graphene oxide–TiO_2 nanocomposites. The composites based device demonstrates photo-sensitive resistive switching characteristics, wherein the forming process can be eliminated with reduced set voltages by controlling the UV irradiation time and TiO_2 particle concentration. More importantly, the switching uniformity and switching speed of the as-fabricated memristor device can be effectively enhanced by the involvement of optical modulation.

Beyond the metal oxide semiconductors, the energy band diagram at two conductive oxide interfaces can also be controlled by optical means. For instance, the Fermi level of the conductive ternary oxide Nb-doped (0.7 wt.%) $SrTiO_3$ is usually below its conduction band. When Nb:$SrTiO_3$ forms a junction with ITO, a Schottky barrier naturally exists at the ITO/Nb:$SrTiO_3$ interface. Gao *et al.* constructed a simple double-layer ITO/Nb:$SrTiO_3$ heterojunction artificial optoelectronic synapse, which shows responses in the entire visible light region (while more sensitive in the short wavelength range) (Fig. 2(d)).[14] Similar to the case of cerium oxide optoelectronic memristors, light illumination will excite and release the electrons trapped at the interface, giving rise to reduced junction barrier height and ITO/Nb:$SrTiO_3$ device transition to the low resistance state.

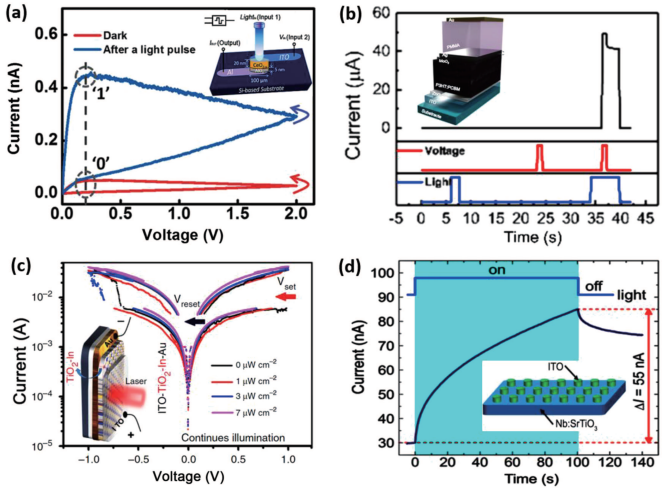


Fig. 2. (a) The resistive switching behaviors of the device before and after light gating in the ITO/CeO_{2-x}/AlO_y/Al optoelectronic memristor.[18] Copyright (2017) American Chemical Society. (b) The process of optical set in a hybrid Au/PMMA/Ag/MoO_3/P_3HT:PCBM/ZnO/ITO device. Inset: Schematic image of the device.[27] Copyright (2019) American Chemical Society. (c) The *I*–*V* curves of Pt/In-doped TiO_2/Au memristor under the continues illumination with different power density. The inset shows the device structure with optical stressing.[29] Copyright (2019) Springer Nature. (d) Current evolution process of the ITO/Nb:$SrTiO_3$ device before and after the light excitation.[14] Copyright (2019) American Chemical Society.

In addition to the above materials, ZnO,[31,32] In_2O_3,[15,33] VO_2,[34] In-Ga-ZnO,[9,35,36] all-inorganic perovskites[37] *et al.* have also been employed as photosensitive materials in optoelectronic memristor systems.

2.2. Organic materials

Most of the work on neuromorphic computing and memory simulation so far has been focusing on inorganic material devices. Theoretically, the change of the intrinsic properties in organic materials will also cause memristive switching for the construction of artificial synapse and neural networks.[38] In comparison with the inorganic counterparts, organic materials have the advantages of low cost, simple processing procedures, good mechanical flexibility and deformability, and the most important of all, the fine-tunability of their electronic properties through molecular design and synthesis.[39]

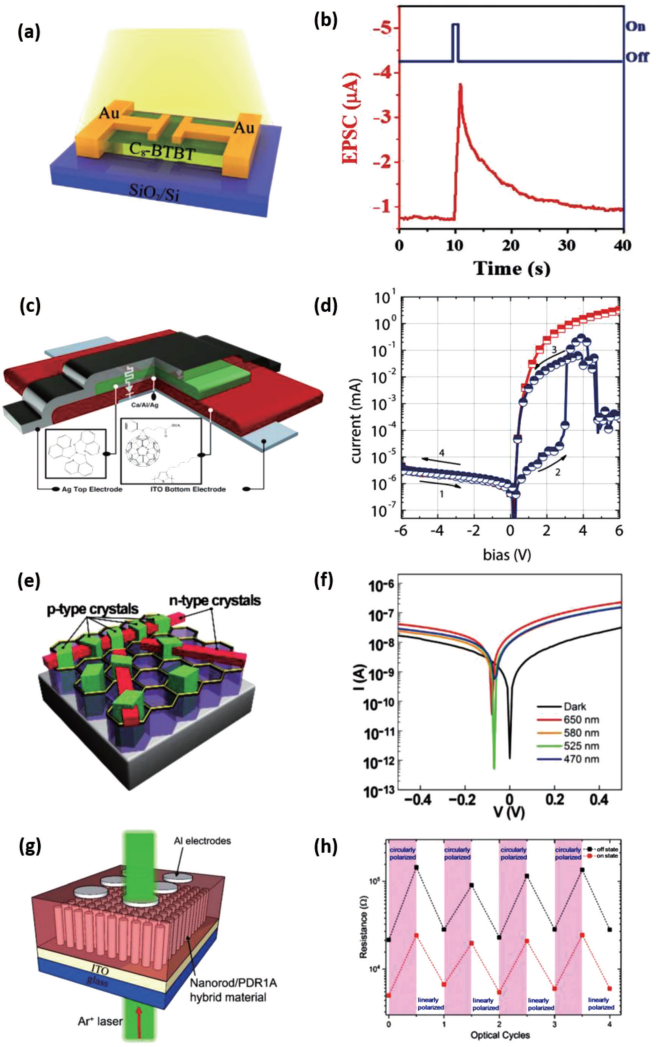


Fig. 3. (a) Schematic diagram of the 2D OSC C8-BTBT-based phototransistor and (b) the change of post-synaptic current under optical illumination.[40] Copyright (2019) John Wiley & Sons, Inc. (c) The structure of P3HT-PCBM based organic photodiode (OPD) device and (d) *I*–*V* curves of the organic resistive switching (ORS, blue) and OPD (red) devices, respectively.[41] Copyright (2015) John Wiley & Sons, Inc. (e) Diagram of the PTCDI-C8/TIPS/PEN based organic photosensitive device and (f) *I*–*V* curves under dark condition and illumination with different light intensities.[42] Copyright (2018) John Wiley & Sons, Inc. (g) Schematic illustration of the ITO/ZnO/PDR1 A/Al optoelectronic memristor and (h) reversible transitions between high resistance state and low resistance state under the circularly and linearly polarized light irradiations.[43] Copyright (2017) John Wiley & Sons, Inc.

Huang *et al.*[40] reported a 2D organic semiconductor (OSC) C8-BTBT synthetized by a solution epitaxy method, the morphology of which is no longer influenced by the underneath substrates. Using C8-BTBT as the semiconductor channel and SiO_2 as the gate insulating layer, a photo-responsible 2D OSC based synaptic transistor was fabricated successfully (Fig. 3(a)). The oxygen-containing polar groups present on the surface of the silicon substrate can serve as interfacial charge trapping centers to affect the carrier transport characteristics. When optical illumination is applied onto the as-fabricated

synaptic transistor, the channel conductance and drain current are significantly modulated (Fig. 3(b)). Both the incoming light intensity and irradiation time can influence the overall device behaviors.

Nau *et al.*[41] designed and fabricated an organic photodiode (OPD), whose resistance was changed with photogenerated charge carriers upon illumination. The photoactive layer of the OPD device is typically a p–n bulk-heterojunction consisted of poly(3-hexylthiophen-2,5-diyl) (rr-P3HT) as the electron donating component and phenyl-C61-butyric acid methyl ester (PCBM) as the electron accepting host, sandwiched between two electrodes (Fig. 3(c)). Two resistance states of the OPD device are clearly distinguished at a low bias, and all the resistance states can maintain when the voltage is removed. Under a bias voltage, the resistive switching phenomenon of the device can be observed after light stimulation (Fig. 3(d)), thereby achieving the combination of organic resistive switching and optoelectronic devices. On the other hand, the easily crystallized organic materials N,N′-dioctyl-3,4,9,10-pe-rylenedicarboximide (usually abbreviated as PTCDI-C8) and 6,13-bis(triisopropylsilylethinyl)pentacene (abbreviated as TIPS-PEN) also show good response to ultraviolet lights. Zhang *et al.*[42] manufactured self-suspended nano-mesh scaffolds on glass and plastic substrates, and asymmetrically connected p–n crystal heterojunctions with optical response characteristics (Figs. 3(e) and 3(f)). Utilizing the unique advantages of organic crystals, the mobility of charge carriers and their transmission distance from where they are generated to that of the electrode position reach the maximum, thereby greatly reducing the light response time.

Beyond small organic molecules, photosensitive polymer materials can also be used as the switching media in optoelectronic memristor devices. Kemp's team demonstrated an optoelectronic memristor, in which the azobenzene based polymer poly(disperse red 1 acrylate), called PDR1 A, is combined with zinc oxide (ZnO) as the active layer in ITO/ZnO/PDR1 A/Al structure devices (Fig. 3(g)).[43] The electrical properties of this combined structure can be controlled by the light (Fig. 3(h)), showing a reversible and latching resistive switching characteristic. By applying a specific polarized light illumination, the distance between ZnO and the electrodes can be changed effectively, which is due to the respective expansion or contraction of the polymer component and will cause variation of the device conductivity. It is noteworthy that the switching voltage remains constant upon optical illumination, and the switching period of the device HRS–LRS transition well follows that of the repeated irradiation with circularly and linearly polarized lights.

2.3. Organic–inorganic halide perovskites

Organic–inorganic halide perovskites (OHPs) are emerging star materials used in optoelectronic memristors in recent years. They have excellent light absorption characteristics, long electron–hole diffusion length, bipolar charge transport, abnormal physical defects, and adjustable band gap. $CH_3NH_3PbI_3$ ($MAPbI_3$) is currently the most representative material in OHPs.[32,44–48] The I^- anions can diffuse spontaneously, which may lead to the iodine defects and influence the stability of the optoelectronic devices. In extreme cases, photovoltaic devices based on $MAPbI_3$ may become short-circuited by I^- migration. To suppress the spontaneous diffusion of I^-, Zhu *et al.* used active metal (such as Ag) as anode materials to form stable AgI_x at the electrode/$MAPbI_3$ interface in Ag/$MAPbI_3$/Au devices (Fig. 4(a)).[49] It is found that the iodine vacancy migration can be obviously influenced by the light. With the increase of the light intensity, the amplitudes of the set and reset voltages decrease and increase, respectively (Fig. 4(b)). They also demonstrate that the $MAPbI_3$-based memristor can exhibit light-tunable synaptic behaviors (Figs. 4(c) and 4(d)), which is attributed to the formation and annihilation of iodine vacancy ($V_I^{\cdot}/V_I^{\times}$) controlled by the light illumination and electric field.[50] The electric field induces the production of $V_I^{\cdot}/V_I^{\times}$, while light inhibits its production and promotes its annihilation. When the electrical bias is removed, light can accelerate the recombination of $V_I^{\cdot}/V_I^{\times}$ with I^-, causing the back transition of the device resistance. As such, through controlling the lighting conditions, suppressed or promoted device conductances can be realized correspondingly.

The optically modulated iodine vacancy movement in OHP based memristor devices was also observed by Wang and coworkers in Ag/$MAPbI_3$/Pt devices (Fig. 4(e)).[51] Considering the photogenerated electric field is produced by the photovoltaic electron–hole separation in perovskite under light illumination, the migration of iodine vacancies will be effectively promoted with the activation energy significantly reduced by the intrinsic potential built between the Ag/$MAPbI_3$ and ITO/$MAPbI_3$ regions. Through the synergetic interplay between the continuous electrical and light stimuli, the postsynaptic current could be effectively controlled (Fig. 4(f)). Furthermore, Zhou *et al.* intentionally introduced Cl^- in $MAPbI_3$ to regulate the formation and crystallization behavior of the perovskite thin film.[52] It is found that both the trap state density and diffusion length of the halide anions can be reduced, which in turn influence the overall electrical properties of the OHP layer. Taking advantage of the unique advantages of $CH_3NH_3PbI_{3-x}Cl_x$, a perovskite-based optoelectronic memristor is demonstrated (Fig. 4(g)). Both the set voltage amplitude and device energy consumption can be significantly reduced by the photo-assisted resistive switching behavior in

$CH_3NH_3PbI_{3-x}Cl_x$ based memristor with optimized film quality (Fig. 4(h)).

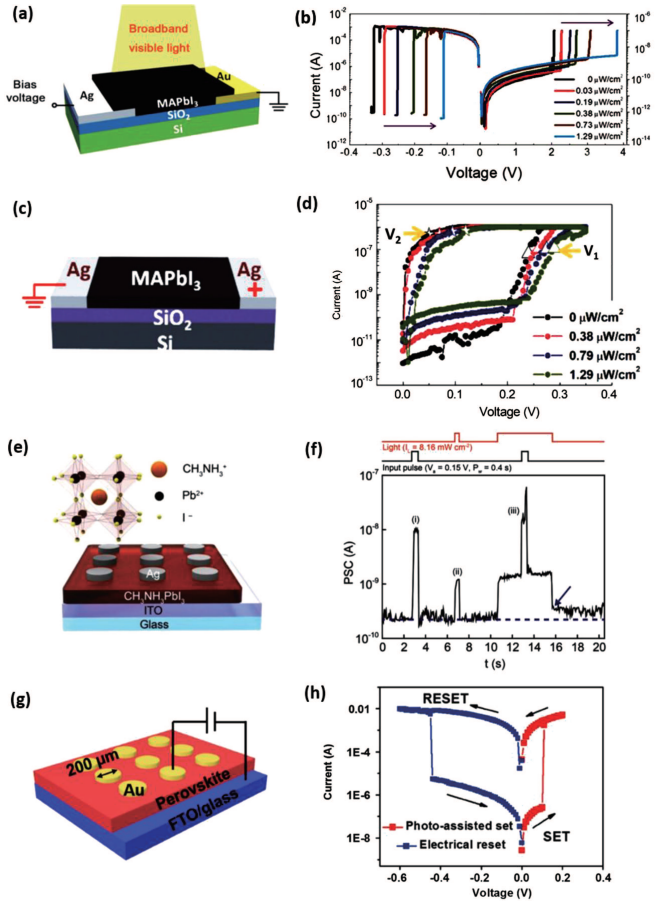


Fig. 4. (a) Schematic diagram of the Ag/$CH_3NH_3PbI_3$/Au device excited by broadband visible light and bias voltage and (b) *I*–*V* characteristics of the set processes with different light illumination intensities. Inset shows the reset processes.[49] Copyright (2017) John Wiley & Sons, Inc. (c) Schematic diagram of the Ag/$MAPbI_3$/Ag device and (d) *I*–*V* curves of the $MAPbI_3$-based memristor measured with different illumination intensities.[50] Copyright (2018) American Chemical Society. (e) Schematics of the Ag/$CH_3NH_3PbI_3$/ITO synaptic device and $CH_3NH_3PbI_3$ structure, (f) the changes of PSC value under the electrical, light, and co-stimulations.[51] Copyright (2019) John Wiley & Sons, Inc. (g) Schematic image of the Au/$MAPbI_{3-x}Cl_x$/ITO memristor and (h) its photo-assisted set and electrical reset processes.[62] Copyright (2018) John Wiley & Sons, Inc.

2.4. Two-dimensional material systems

Due to their ultra-thin structure and large specific surface area with high sensitivity to subtle changes happened in the local environment,[53–55] two-dimensional materials (especially their device electrical response characteristics) are very sensitive to the photo-excited charge detrapping processes.[56–59] With the rapid responding speed, multi-level switching potential, large ON/OFF ratio of the as-obtained photocurrent or photoconductivity,[60–62] 2D materials and their heterojunctions are promising candidates in optical sensing, data storage and processing, and neuromorphic computing applications.

So far, graphene, hexagonal boron nitride (h-BN), transition metal dichalcogenides (TMDs), and their heterojunctions have been widely used in optoelectronic synaptic devices.[63–69] For example, the monolayer MoS_2 with direct band gap shows strong response to light irradiation. Utilizing the characteristics, Lee *et al.* designed a single-layer MoS_2 based optoelectronic device for image sensing and detection (Fig. 5(a)).[70] Based on the charge trapping at the MoS_2/SiO_2 interface and subsequent light-induced charge release, the device current decreases obviously with increasing in the optical illumination time (Fig. 5(b)). By modifying the interface with functional groups to enable the controlled capture and release of charges upon electron localization, higher linear response range, larger ON/OFF ratio, and lower power consumption can be achieved in the devices. Cho prepared an optoelectronic transistor with MoS_2 as the channel and light absorption layer, and Au deposited in the form of nanoparticles (NPs) as the charge trapping layer (Fig. 5(c)).[71] Due to the direct band gap of MoS_2, the drain current of the device shows an obvious dependence on the illumination light wavelength (Fig. 5(d)). Electrons are excited from the valence band to the conduction band of MoS_2 continuously, which causes significant enhancement in the drain current as plotted and consequently multilevel modulation characteristics. More importantly, the application of negative gate voltage can lead to charge migration from the Au nanoparticle layers into the valence band of the MoS_2 layer. This would prohibit the recombination of the photo-excited electron with valence band vacancy, giving rise to prolonged life time of the photocurrent signal and thus nonvolatile nature for data storage. By adjusting the amplitude of the applied voltage and the light illumination intensities, continuous modulation of the device drain current also allows the integration of optical signal processing capability in the MoS_2 based transistor optoelectronic devices.

In addition to the single component 2D materials, the van der Waals heterojunctions of multiple low-dimensional materials with different chemical, physical, and electronic characteristics can provide extra possibilities for more complex optoelectronic performances. Qin *et al.* first reported an optoelectronic random-access memory synaptic device based on graphene–carbon nanotubes (CNT) composite.[72] The conductance of the channel layer can be regulated by the light and electrical pulses, wherein the short-term synaptic plasticity (STP) is achieved by charge transfer between the graphene and carbon nanotubes species. With different gate voltages, the plasticity is flexibly regulated to get dynamic synapses with tunable weight. Lee *et al.*[69] reported a multilevel nonvolatile optical memory device based on the MoS_2/h-BN/graphene heterostructure (Fig. 5(e)). The monolayer MoS_2, the graphene, and the h-BN were used as the light absorbing layer, floating gate, and dielectric tunneling layer, respectively. Under dark conditions, applying sweeping source–drain voltage (V_{DS}) from −10 V to 3 V, I_{DS} dropped to 10^{-14}

at the read voltage of 0.5 V (Fig. 5(f)) due to electrons being confined in the graphene floating gate by tunneling through the h-BN barrier at the higher negative voltage bias. However, upon the light pulses, the photogenerated holes in the MoS_2 channel can tunnel through the h-BN layer to neutralize the restricted electrons in graphene, which leads to the current sharply increase (Fig. 5(f)). The current switching ratio current can be modulated by light intensity. Furthermore, the photo induced current changing was nonvolatile. In addition, Xiang reported multi-bit nonvolatile optoelectronic memristor in Au/WSe_2/BN/Au structures (Fig. 5(g)), in which the storage current can be jointly adjusted through electrical and optical modulations.[73] In the programming process, the photo-excited electrons are transferred from BN into WSe_2, while the local positive charges are stored in the band gap of BN by the negative gate voltage. During erasing, the positive gate voltage can extract the photo-excited electrons from the WSe_2 channel back to the BN layer and restore the initial transport characteristics of WSe_2. In addition, they found that the WSe_2/BN heterostructure has a significant wavelength dependence in the entire visible spectrum (Fig. 5(h)), so that it can be used as a color image sensor without filters.

Beyond the above optoelectronic memristive materials, zero-dimensional quantum dots with unique edge effects are also used for optoelectronic memristors applications.[74–76] As compared with transition metal dioxides, the complex oxide systems generally need high temperature fabrication process, which is incompatible with the CMOS technology. In the meantime, an indirect band gap of these complex oxides is disadvantageous for optimizing the photoelectrical responses of the as-obtained devices. Thus, searching for dioxides with direct band gap and optimal optical-electrical characteristics could be a promising direction for the development of oxide based optoelectronic memristors. On the other hand, although perovskites exhibit excellent photo response, the poor air-humidity of this new class of organic–inorganic hybrid stability arises the critical hinderance that restricts their direct device applications. In recent years, due to the great potential in energy consumption reduction, the high-density integration ability, and the sizable photo response in a wide spectra range, 2D materials have drawn great attention and have been intensively investigated. However, the production of large area and high-quality 2D membrane is only restricted to a few materials, the growth recipe of 2D materials with large area and high quality needs to be further explored. Although there exist plenty of material candidates showing potential for future optoelectronic memristor and neuromorphic computing applications, great amount of efforts are still highly desired to overcome the scientific and technological problems before making real advancements in this particularly interesting area.

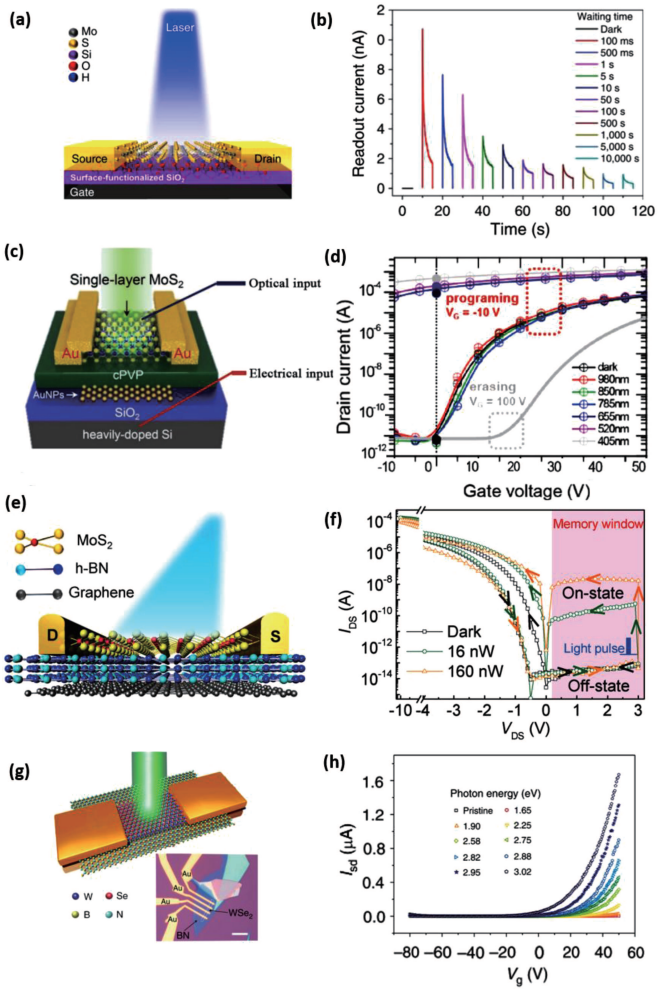


Fig. 5. (a) Schematic diagram of an optoelectronic memristor based on silanol groups functionalized MoS_2/SiO_2 interface and (b) the relationship between read current and different light illumination durations.[70] Copyright (2017) Springer Nature. (c) The structure of single layer MoS_2 based optoelectronic memory device and (d) the evolution of the device current upon photo illuminations with various wavelengths.[71] Copyright (2016) John Wiley & Sons, Inc. (e) Schematic structure of an optical memristor based on the heterojunction of the MoS_2/h-BN/graphene, (f) The I_{DS}–V_{DS} curves of the device obtained with and without light pulses.[69] Copyright (2019) John Wiley & Sons, Inc. (g) Schematic illustration of the WSe_2/BN heterostructure-based optoelectronic memory. Inset: optical image of the device. The scale bar is 10 μm. (h) Evolution of the device current obtained under illumination at various light intensities.[73] Copyright (2018) Springer Nature.

3. Working mechanisms of light-modulated memristor devices

Switching mechanisms of the memristor include the ion-migration with redox processes inducing the growth and dissolution of filaments[11,77] and the regulation of the interface barrier between electrodes and dielectric layer.[20,78] Therefore, memristor characteristics can be well modulated through photo-assisted ions diffusion, chemical reaction in solid films, and photo-modulated interface barrier.[17,26,79]

3.1. Optically modulated interface barrier

Resistance of memristors can be optically modulated by changing the Fermi level of the switching materials and

the interfacial Schottky barrier formed between the electrode and the dielectric layer.[31,80,81] As discussed previously, Tan *et al.*[17,18] designed a $CeO_{2-x}/AlO_y/Al$ junction, in which charge trapping sites are formed at the interface between the cerium oxide and the natively oxidized aluminum oxide layers (Figs. 6(a) and 6(b)). When the optical illumination is applied, the electrons of the trapping sites are excited and move away from the interfacial region under the electric field. The positively charged oxygen vacancies (V_o^{2+}) left behind intensify the band bending at the $CeO_{2-x}/AlO_y/Al$ interface and thin down the Schottky barrier width. Consequently, the charge carrier transport across the junction is promoted significantly, giving rise to photoconductivity in ITO/CeO_{2-x}/AlO_y/Al device. The application of negative voltage can drive the electrons back to the $CeO_{2-x}/AlO_y/Al$ interfacial trapping sites, recovering the initial energy band and switching the device back to the initial low conductivity state. In Zhou's work,[52] it is revealed that the photogenerated holes can be trapped by the hole trapping centers located at the interface between the perovskite and Au (Fig. 6(c)), which would shift the Fermi level of the perovskite toward the valence band and decrease the Schottky barrier. In such a case, a small bias (0.1 V) can switch the device from the initial high resistance state into a low resistance state under light illumination, which will ultimately lower the energy consumption of the photo-assisted memristor with low programming voltages. Gao *et al.*[14] also explained a mechanism of Schottky barrier regulation by light and electric field at the ITO/Nb:$SrTiO_3$ interface (Fig. 6(d)).

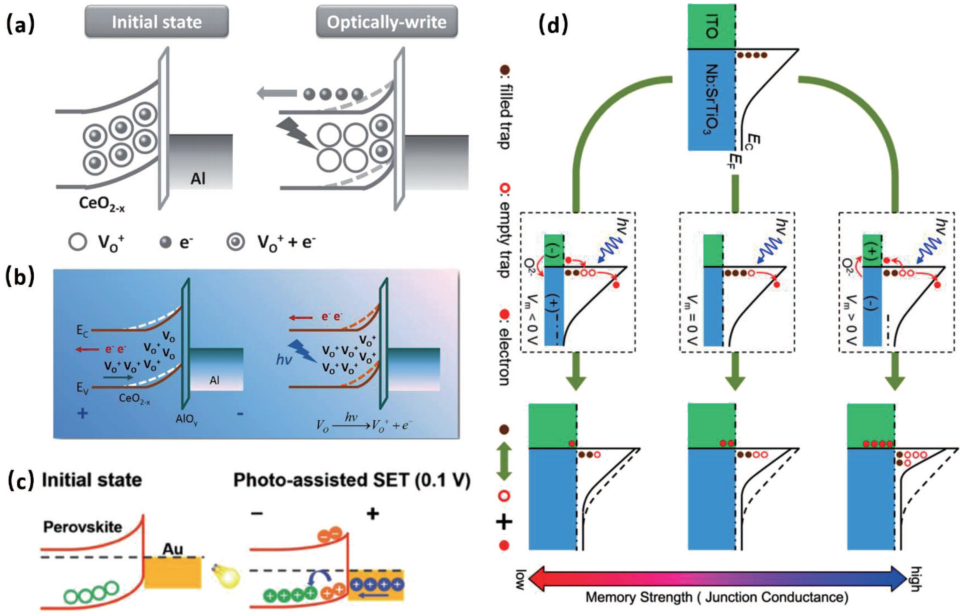


Fig. 6. (a) Schematic illustration of the energy band diagram of the $CeO_{2-x}/AlO_y/Al$ junction under optical illumination stimulation.[17] Copyright (2015) John Wiley & Sons, Inc. (b) Mechanism of the ITO/CeO_{2-x}/AlO_y/Al optoelectronic memristor through light modulating.[18] Copyright (2017) American Chemical Society. (c) Photo-assisted shifting of perovskite Fermi level towards the valence band by hole trapping at interfacial trap sites.[52] Copyright (2018) John Wiley & Sons, Inc. (d) Schottky barrier profiles after light illumination and voltage stressing at the ITO/Nb:$SrTiO_3$ heterojunction.[14] Copyright (2019) American Chemical Society.

3.2. Light induced molecular isomerization

In some organic or hybrid organic–inorganic memristors, optical illumination can induce isomerization of the organic molecules, which in turn will lead to tuning of the device conductance.[82–85] Jaafar reported that in a photoactive azobenzene polymer based memristor device, irradiation with polarized light results in expansion (by circularly polarized light beam) or contraction (by linearly polarized light beam) of the azobenzene polymer (Fig. 7(a)).[82] Circularly polarized light beam can align the azobenzene chromophores of the polymer in the direction of its polarization, while linearly polarized light beam will switch the alignment of the azobenzene chromophores to the opposite direction.

Qiu and coworkers designed a hybrid structure memory by combining photo-responsive diarylethene (DAE) molecule with semiconducting 2D materials (2DMs).[86] Through the reversible photochemical isomerization (open (DAE_o) and closed (DAE_c) isomer) of the DAEs under UV and visible light illumination, the molecular orbital energy levels and consequently the charge carrier transport across the underneath 2DMs (WSe_2 and black phosphorus) can be effectively modulated. As shown in the energy-level alignment of WSe_2/DAE_1, BP/DAE_2, and BP/DAE_3 in Figs. 7(c) and 7(d), the conduction band minimum (CBM) of the n-doped WSe_2 is below the lowest unoccupied molecular orbital (LUMO) levels of DAE_1o and above the LUMO levels of DAE_1c, thus the electrons transfer from WSe_2 to DAE_1c will result in a decrease of the electron density. For the p-type BP, the valance band maximum (VBM) is located between the the highest occupied molecular orbital (HOMO) lev-

els of DAE_2o and DAE_2c, thus the holes transfer from BP to DAE_2c will lead to a decrease of the hole density. For BP/DAE_3, due to the HOMO of DAE_3c being similar to the VBM of BP, the charge density will be unchanged. Therefore, it is a suitable way to realize light modulated resistance change of memristors by combining photosensitive molecule decorated 2D materials that can achieve fast, noninvasive, and easily addressable light triggering. These hybrid optoelectronic memristors can be used as nonvolatile multilevel memories (Fig. (7e)).

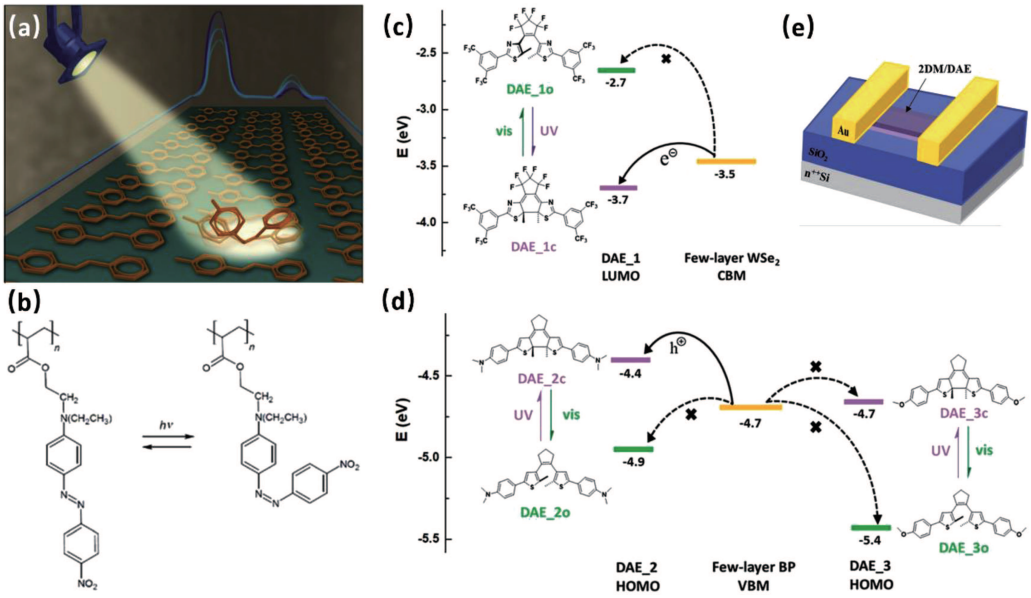


Fig. 7. Photo inducing isomerization of (a), (b) the azobenzene polymer[82,84] and (c), (d) diarylethenes molecules.[86] Copyright (2012) Royal Society of Chemistry, Copyright (2006) American Chemical Society, and Copyright (2019) John Wiley & Sons, Inc. (e) Device structure of optoelectronic memristor based DAE decorated 2D materials.[86] Copyright (2019) John Wiley & Sons, Inc.

3.3. Photo-assisted ion diffusion and electrochemical reaction

As in the case of electro-catalysis, light illumination can assist the diffusion of vacancy and ionic species in the memristors.[44,87,88] Zhu found that under the bias, the visible light illumination can inhibit the formation of $V_i^{\cdot}/V_i^{\times}$ or V_I-rich CFs while facilitate the annihilation of $V_i^{\cdot}/V_i^{\times}$ in the $MAPbI_3$-based memristor (Figs. 8(a)–8(c)).[49,50] In the meanwhile, the switching voltages and the retention performance of the resistance states can also be affected by the irradiating light beams. These phenomena were also certified by de Quilettes *et al.* through the time-of-flight secondary-ion-mass spectrometry (ToF-SIMS) depth profiling on the photo-excited $CH_3NH_3PbI_3$ films. Non-uniform distribution of the iodide signal at the photo-illuminated region is shown in Fig. 8(d). Figure 8(e) shows the regions of highest illumination intensity (from blue line) corresponding to the lesser iodide, while the vicinity regions exhibit an enrichment of iodide, suggesting that the photo-induced iodine lateral migration away from the illumination area happens (Figs. 8(d) and 8(e)).

Different from photo-generated electron and hole carriers in the small bandgap dielectrics, Zhou and co-workers reported that optical illumination can also induce the excitation of oxygen ions in large bandgap HfO_2 (SiO_2)-based memristors, wherein the migration of the mobile oxygen ions and their recombination with the oxygen vacancies will lead to the formation of CF and thus negative photoconductivity (NP) characteristic.[89,90] In addition, the conductance of the light-modulated memristor depends on the diameter of the filament received at different current compliance (CCL) limit levels. Figure 8(f) shows that the voltage applied by the conductive atomic force microscope (C-AFM) tip can induce the formation of a thinner oxygen-deficient filament in the HfO_2 dielectric with interstitial oxygen ions under low CCL. When white light illumination is applied onto the device, the incident photons would drive the adjacent interstitial oxygen ions towards the vacancy-rich filament (Fig. 8(g)) and annihilate the filament. Under a larger CCL, stronger filament will be formed while the neighboring interstitial oxygen ion concentration is much lower (Fig. 8(h)). Application of light irradiation can only activate fewer interstitial oxygen ions reaching the filament and partially disrupt the filament. Although the incident light can also stimulate lattice oxygen ions to recombine with the filament vacancies, removal of the optical illumination will lead to the relaxation of the activated oxygen ions to their initial lattice occupation (Fig. 8(i)). Metallic Ag based CFs and quantum point contacts are also responsive to the optical illumination for light-induced low to high resistance state transition for optoelectronic memristor applications.[91,92]

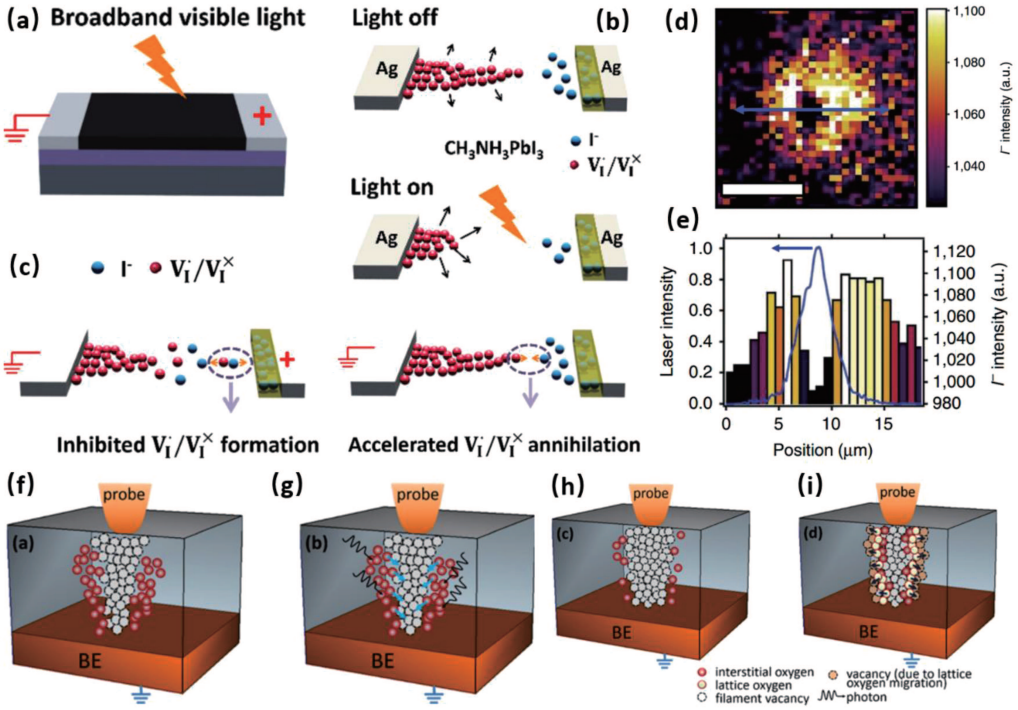


Fig. 8. (a) Schematic illustration of the $MAPbI_3$ memristor illuminated by broadband visible light. (b) Formation and inhibited growth of CF during light stressing and removal, respectively. (c) Inhibiting formation (left) and accelerating annihilation (right) of CFs under light illumination.[50] Copyright (2018) American Chemical Society. (d) ToF-SIMS image of the iodide distribution in light-illuminated region. (e) Iodide distribution (right axis) in line scan area of the blue arrow in (d) and spatial profile of the illumination (blue line) (left axis).[87] Copyright (2016) Springer Nature. (f) The formation of thinner oxygen vacancy filament and the interstitial oxygen ions released in the neighborhood of the filament with low compliance current level (CCL). (g) Disruption of filament by photo-excited interstitial oxygen ions migration to recombine with the filament vacancies. (h) Formation of the stronger filament at a higher CCL with fewer interstitial oxygen. (i) Partial disruption of filament due to limited supply of photo-excited migration of interstitial and lattice oxygen ions.[89] Copyright (2015) AIP Publishing LLC.

With the participation of proton in electrochemical reaction processes, the introduction of light onto memristive switching media can also lead to the change of valance state of the constituting elements. Upon the generation of protons from the environmental water by optical illumination, Zhou *et al.* demonstrated that a change of Mo ion valence state from 6^+ to 5^+ in the MoO_x thin film can result in the transition of resistance states from HRS to LRS, accompanied by the color change of the thin film from transparent to blue of the hydrogen molybdenum bronze (H_yMoO_x) species.[26] The reaction formulas, involving the photogenerated electrons (electrons being excited to the conduction band of MoO_x) and the protons (protons being produced through the holes reacting with the absorbed water molecules in the MoO_x thin films),[93,94] are listed as follows:

$$MoO_x + h\nu \rightarrow MoO_x^* + e^- + h^+, \quad (1)$$

$$4h^+ + 2H_2O \rightarrow 4H^+ + O_2, \quad (2)$$

$$MoO_x + ye^- + yH^+ \leftrightarrow H_yMoO_x. \quad (3)$$

They also carried out x-ray photoelectron spectroscopy (XPS) measurement to confirm the change of the Mo cation valence state upon the light irradiation, and obtained the Mo 3d XPS spectra of MoO_x before and after the UV illumination, respectively. Before optical illumination, the MoO_x film shows Mo^{6+} $3d_{3/2}$ peak at the binding energy of 236.0 eV and Mo^{6+} $3d_{5/2}$ peak at 232.9 eV, respectively. After UV illumination, Mo^{5+} $3d_{3/2}$ (234.9 eV) and Mo^{5+} $3d_{5/2}$ (231.8 eV) appear, assuring the valence change of Mo^{6+} to Mo^{5+} upon UV illumination on the MoO_x thin film and the formation of new phase H_yMoO_x.

Chen *et al.* displayed an artificial visual system constructed from a serial of a photosensitive image sensor and a resistive switching memory device (Fig. 9).[4] Resistances of the underneath memory layer are modulated by the incident UV light that stimulates the image sensor and results in the changing of the voltage drop on the memory. Without any optical illumination, the resistance of the image sensor is larger than that of the memory layer. The partial voltage drop on the memory device is unable to switch it from HRS to LRS, thus no optical signals are detected nor stored. When UV beams are illuminated onto the sensor layer, the sensor resistance will be decreased by photon excitation, whereas the increased partial voltage shared by the memory will switch it from HRS to LRS nonvolatilly, which is due to the formation of Ni filament by electrochemical reaction.[95,96] Afterwards, an opposite voltage can dissolute the filament and reprogram the memory back to the initial HRS state.

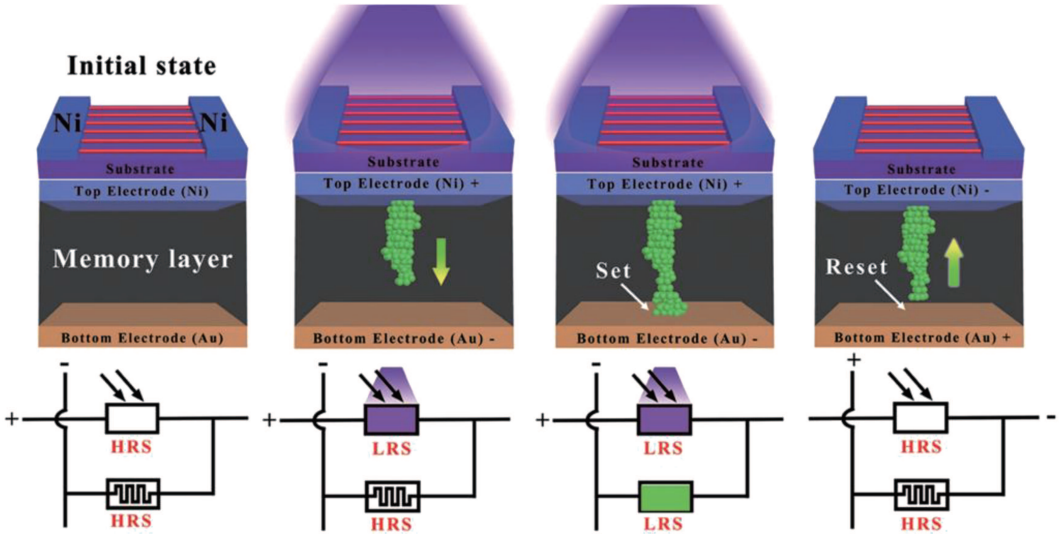


Fig. 9. Schematic illustrations of working mechanism of an artificial visual system constructed from a serial of a photosensitive image sensor and a resistive switching memory device.[15] Copyright (2018) John Wiley & Sons, Inc.

4. Applications of optoelectronic memristors

Optoelectronic memristors, whose conductance can be co-regulated by optical and electric means, have many applications including optogenetics synaptic plasticity and brain-inspired computing, efficient neuromorphic visual systems, arithmetic computing, acceleration and artificial nociceptor, etc. The following section will discuss the recent advances in the applications of optoelectronic memristors.

4.1. Optoelectronic artificial synapses

As the next-generation computing for beyond von Neuman architecture, artificial synapse-based neuromorphic computing can merge the central processing unit and the memory hierarchy in a single integrated circuit chip, therefore eliminating the data transfer bottleneck for high efficiency computing. Generally, a synapse is a bridge that connects the pre- and post-neurons. Pre-neuron generates action potentials that can propagate to the next neuron and induces the postsynaptic action potentials (Fig. 10(a)).[97] Synaptic weight represents the communication strength of the connection between the pre- and post-neurons, while the synapse can compute and learn by strengthening or weakening the connection strength between two neurons. The neuronal activities can be controlled with precise temporal and spatial modulation in neural systems. In optogenetics, the excitation or inhibition of the neuron can be achieved by light stimulation with different wavelengths to activate/deactivate the ion channels with varying membrane potentials (Fig. 10(b)).[98] The optoelectronic memristors, with lowered energy consumption by a spatially separated stimulus, resemble optogenetics in kinetic processes and are feasible candidates to nondestructively simulate the optogenetics-mediated synaptic functions. As four forms of synaptic plasticity, spike-timing-dependent plasticity (STDP), spike-rate-dependent plasticity (SRDP), short-term plasticity (STP), long-term potentiation (LTP), and long-term depression (LTD) can be modulated by the optoelectronic memristors. The synaptic weight change (ΔS) is controlled through light spike wavelength (Fig. 10(c)),[99] intervals (Fig. 10(d)),[29] intensity (Fig. 10(e)),[80] or number (Fig. 10(f)).[68] The ΔS increases with the increase of the spike number, wavelength, and intensity which is owning to the photogenerated electrons and holes and implies a STP to LTP transition. This transition can also be achieved via increasing the pulse width.[40] Another case is the generation of higher excitatory postsynaptic current (EPSC) with lower light stimulation frequencies (Fig. 10(g)),[100] which can be used for low-pass filtering. The STDP is represented by ΔS between the presynaptic and postsynaptic spikes with an interval time of Δt. With the same wavelength, ΔS shows a symmetric Hebbian learning rule at $\Delta t = 0$.[64] Both the ultraviolet visible,[17,18,80] infrared,[99] and the full-spectrum lights[64] can stimulate the optoelectronic memristors to emulate the fundamental STP, LTP, paired-pulse facilitation (PPF), and paired pulse depression (PPD) synaptic functions. Besides, different polarized lights can also enable the weakening or strengthening of the synaptic connections. The repeated circularly polarized pulsed-light will lead to decrease in conductance for emulating the neuromorphic depression and linearly polarized light is used for simulating the neuromorphic potentiation (Fig. 10(h)).[43] These results illustrate that optoelectronic memristors are capable of mimicking fundamental synaptic functions under external light signals.

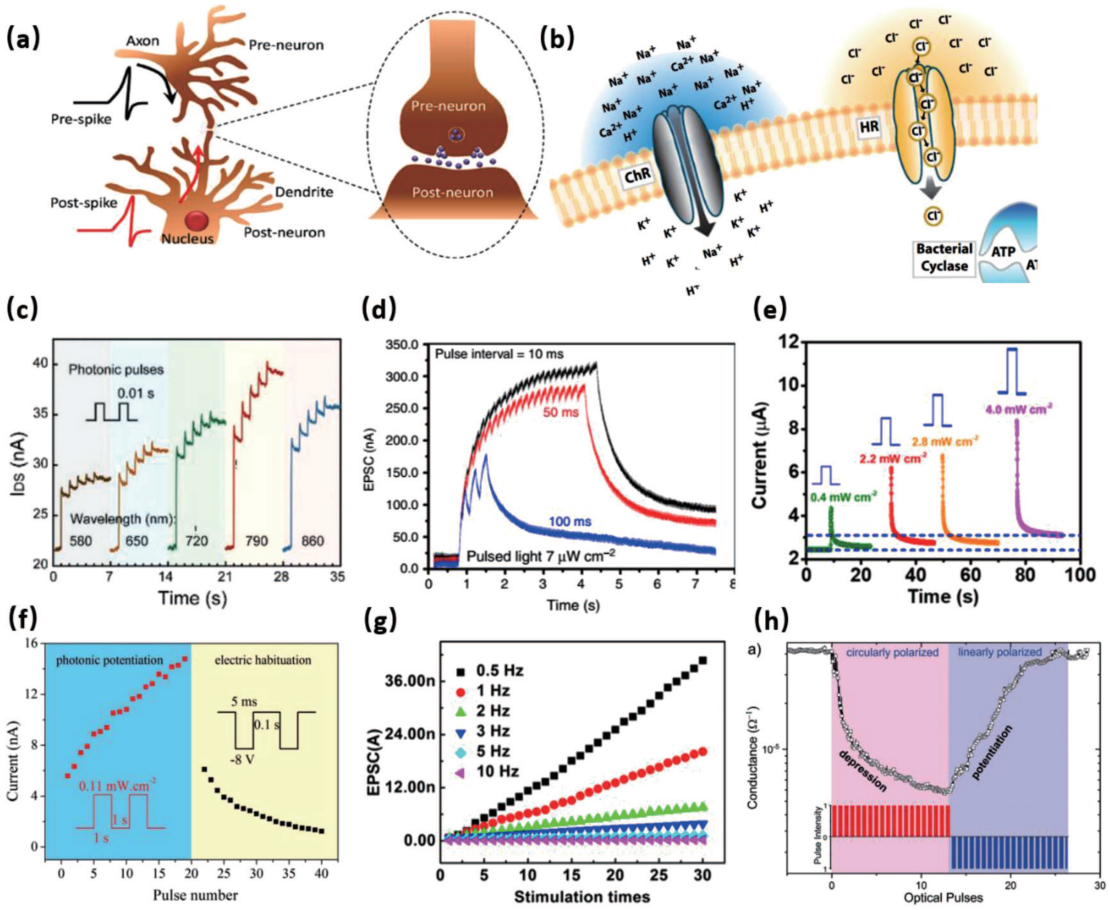


Fig. 10. (a) Schematic diagram of signal transmission between pre-synaptic neuron and post-synaptic neuron by a connected biological synapse.[97] Copyright (2016) John Wiley & Sons, Inc. (b) Diagrams of ion transport under light excitation in optogenetics.[98] Copyright (2011) Elsevier Inc. (c) Dependence of the synaptic weight on the (c) wavelength,[99] (d) interval,[29] and (e) intensity[80] of light spikes. Copyright (2019) John Wiley & Sons, Inc, Copyright (2018) Springer Nature and Copyright (2018) American Chemical Society. (f) Photonic potentiation and electric habituation.[68] Copyright (2018) John Wiley & Sons, Inc. (g) The dependence of EPSCs on the different light stimulation frequencies.[100] Copyright (2019) American Chemical Society. (h) Habituation controlled by different polarized lights including circular and linear polarizations.[43] Copyright (2017) Royal Society of Chemistry.

4.2. Image recognition

One of the potential applications of the optical neural network is image processing (also known as pattern recognition tasks). In conventional image processing task, the optical signals in the images are converted to electronic signals before neuromorphic computing. For example, Chen and coworkers integrated In_2O_3-based image sensors with Al_2O_3-based memristors to realize the image sensing and memristor processing toward artificial visual memory.[15] As a forward step, optoelectronic memristors offer a light-involved tuning of synaptic weight, which is advantageous in lower energy consumption and faster processing time. Ham *et al.* constructed a two-terminal perovskite-based optoelectronic artificial synapse, where light illumination facilitated the iodine vacancies movement in the perovskite layer, resulting in easier realization of LTP.[51] To demonstrate the pattern recognition ability, a pattern "3" is input into a neural network composed of 28 by 28 input and 10 output neurons between which are individual synapses with different synaptic weights for recognition (Fig. 11(a)). After updating the weight, the fully trained artificial network is able to execute the recognition process of input patterns. They demonstrated a high pattern recognition rate of more than 80% after limited learning phases with light illumination. The recognition accuracy 82.7% is much higher than that achieved by solely using smaller voltage excitations (10.29%) (Fig. 11(b)). The energy consumption (4.82 nW for initial update in potentiation) is also lower than that (12.80 μW) of the larger voltage excitation for reaching similar recognition accuracy. Figure 11(c) shows the recognized images in different cases, indicating the larger conductance values (μS) arising under the light-assisted and larger voltage exciting conditions with the higher recognition accuracies. Increasing the light frequency and the number of conductance states could further improve the recognition accuracy.

Moreover, by implementing synaptic and optical-sensing functions together on a van der Waals heterostructure, Seo demonstrated an optic-neural synaptic device that is able to recognize the target colored number from 28 by 28 RGB-colored images (similar to a color-blindness test).[63] They compared two separate neural networks (Fig. 11(d)). In the conventional neural network (NN), the input layer is consisted of neuron arrays with the color-filtering function to emulate the biological cone cells of the human vision system, but the

synaptic connections are formed without the optical-sensing function. In the optic-neural network (ONN), an optical-sensing function is added to the synaptic connection. They found that after the 50th epoch, the recognition rate for mixed-color digits (Fig. 11(e)) of the ONN exceeds 90%, while that of the NN is below 40%. These results demonstrate that an accurate color-mixed pattern recognition can be achieved in ONNs.

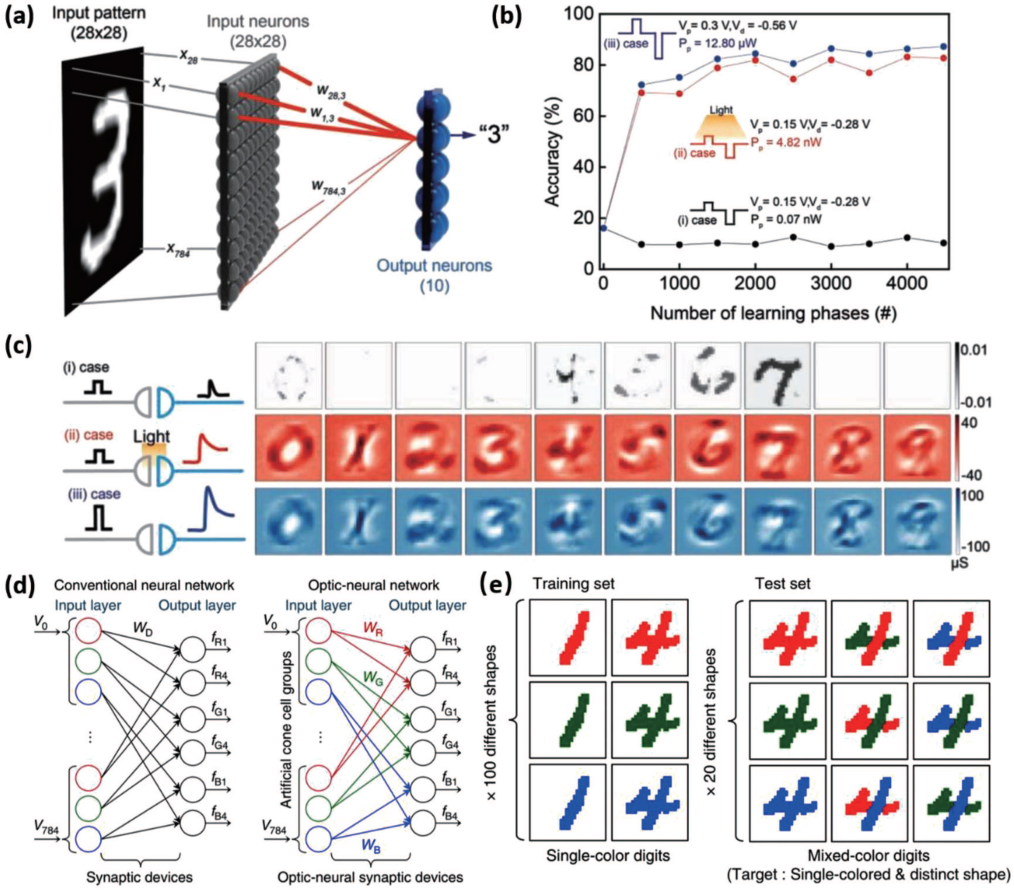


Fig. 11. (a) A single-layer artificial neural network composed of 784 input and 10 output neurons, jointed by independent synapse with different synaptic weight. Each input neuron corresponds to a pixel of the input pattern. (b), (c) Comparisons of the image recognition accuracy at different optoelectronic cases.[51] Copyright (2019) John Wiley & Sons, Inc. (d) Optic-neural network for recognition of 28 by 28 RGB-colored images. (e) Examples of the training and the testing datasets consisting of single-colored and color-mixed numeric pattern images, respectively.[63] Copyright (2018) Springer Nature.

4.3. Efficient neuromorphic visual systems

As nearly 80% of the information that one human being receives is obtained through visual perception, it is necessary to emulate the neuromorphic visual systems with integrated sensor, data storage, and processing functions through optoelectronic memristors.[101,102] Gao and co-workers demonstrated an artificial optoelectronic synapse that is suitable for the mimicry of interest-modulated human visual memories, resembling the function of iris in human eyes.[14] This is realized through the light and electric field co-modulation of the Schottky barrier at the ITO/Nb:$SrTiO_3$ interface, where a positive voltage bias is found to enhance the photo-responsive efficiency while a negative voltage bias will suppress the photo-responsiveness. The photo-response behaves in a neuromorphic manner, while the voltage bias could represent different level of interest. Assuming that a person has low, intermediate, and high interests to the letters L, I, and H after an identical exposure time, the artificial optoelectronic memristive synapses corresponding to these letters would output low, intermediate, and high currents, respectively (Fig. 12(a)). Similar results were also found by Zhou *et al.*[26] Furthermore, neuromorphic preprocessing by an optoelectronic memristor before the image recognition can improve the image recognition rate. The letters P, U, and C with the dimensions of 6×7 pixels are highlighted with the smooth background noise during preprocessing, wherein the preprocessed images are faster recognized with a recognition rate of 0.986 in comparison with that without preprocessing (2000 training epochs are needed to reach the recognition rate of 0.980). At the device level, the memory arrays consisting of 10×10 pixels designed by Chen *et al.* show the capability of sensing and recording the information of a butterfly-shaped image pattern (Figs. 12(b) and 12(c)).[15]

In addition to the visual recognition and memory system, artificial optoelectronic nociceptors that alert us to potential damage from extreme illuminations have also been proposed. Kumar demonstrated a highly transparent artificial photonic nociceptor which is constructed by an antimony-

doped tin oxide (ATO) layer, sandwiched between ZnO and fluorine-doped tin oxide (FTO).[31] As a result of the charge trapping/detrapping at the ZnO/ATO interface, the device exhibits a loop opening in the *I*–*V* characteristics and an optically trigged nociceptive behavior (Fig. 12(d)). Versatile criteria of a nociceptor, such as a threshold, relaxation, allodynia, and hyperalgesia have been demonstrated under self-biased condition (Fig. 12(e)), offering potential in mimicking complex behavior with simple structures and high energy efficiency in future electronic eye applications.

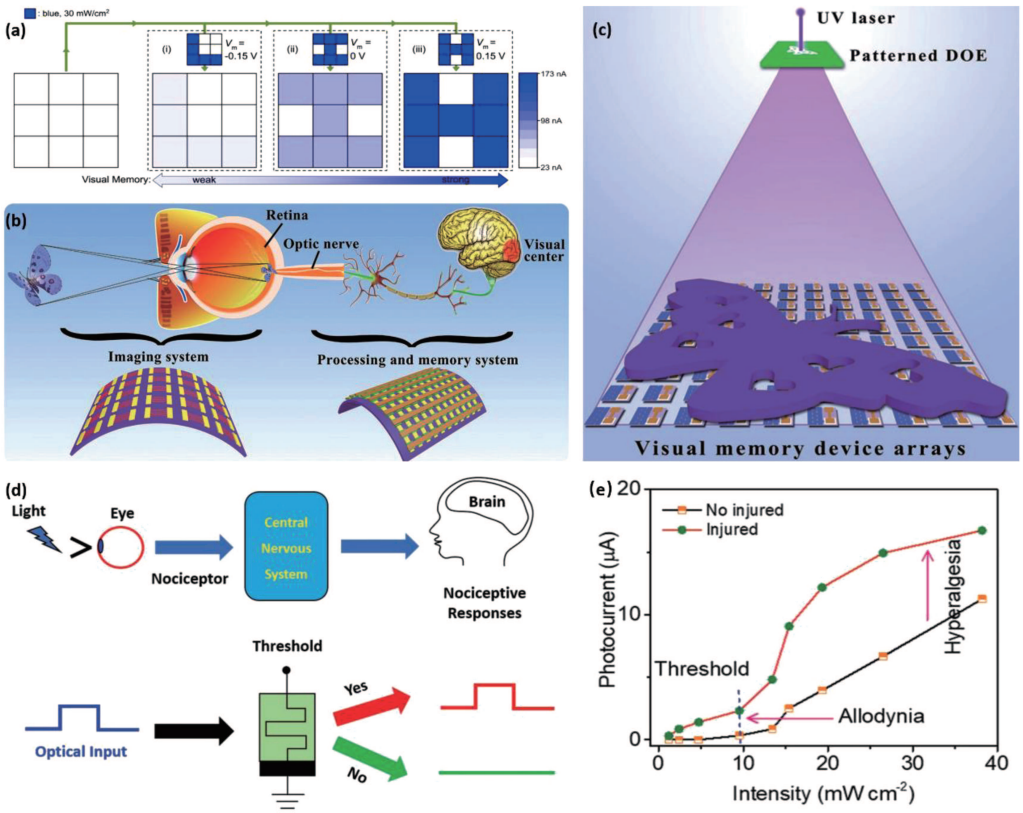


Fig. 12. (a) The mimicry of interest-modulated human visual memory with (i) low interest represented by $V_m = -0.15$ V, (ii) intermediate interest represented by $V_m = 0$ V, and (iii) high interest represented by $V_m = 0.15$ V.[14] Copyright (2019) American Chemical Society. (b) Schematic diagrams of a butterfly being observed through human visual system and (c) schematic diagram of the artificial visual memory devices for detecting and storing image.[15] Copyright (2018) John Wiley & Sons, Inc. (d) Working mechanism of the human eye and threshold-intensity-dependent photo-response of the photodetector. (e) Experimentally measured photocurrent of the device before and after the UV illumination, showing the appearance of allodynia and hyperalgesia characteristics.[31] Copyright (2019) John Wiley & Sons, Inc.

5. Conclusion, challenge, and prospective

Optoelectronic memristor, being sensitive to light, has been extensively studied with a variety of material systems, working mechanisms, and applications. In this review, we firstly summarize the materials systems of optoelectronic memristor including metal oxide semiconductor, organic materials, organic–inorganic halide perovskites, and 2D materials. Then, the working mechanisms of optoelectronic memristor, including the photo-modulated interface barrier, light-excited molecular isomerization, and photo-assisted ions diffusion and electrochemical reactions, are discussed. Lastly, applications of the optoelectronic memristor in artificial synaptic emulation, image recognition, and neuromorphic visual system are stated. Optoelectronic memristors inherit the potential capability of neuromorphic computing through artificial neural network (ANN) algorithms that conventional memristive devices have demonstrated in the past decade, while offer additional figures of merit of extra modulation methods and possibility of function integration of image formation and recognition in a single system. Although great progress has been made in the field of optoelectronic memristor in the past decade, some important challenges, including obtaining more conductance states with photo-electric linear regulation, realizing reconfigurable neural network systems in hardware devices, and mimicking the brain's complex functions in an efficient way, need to be overcome. Thus, in the future, further comprehensive understanding the working mechanism of the optoelectronic memristor, exploring new proof-of-concept optoelectronic materials and architectures with a continuously variable synaptic plasticity for efficient neuromorphic computing, developing ultra-fast optoelectronic memristors and relative testing tools, expanding their applications in human–computer interaction (e.g., neuromorphic robotics), constructing flexible and transparent optoelectronic memristors for simulating more complex retinal functions, and emulating more

receptors including auditory and olfactory should be carried out to broaden the application scenario of the optoelectronic memristor devices.

References

[1] Waldrop M M 2016 *Nature* **530** 144
[2] Hasegawa T, Terabe K, Tsuruoka T and Aono M 2012 *Adv. Mater.* **24** 252
[3] Lee J and Lu W D 2018 *Adv. Mater.* **30** 1702770
[4] Tang J, Yuan F, Shen X, Wang Z, Rao M, He Y, Sun Y, Li X, Zhang W, Li Y, Gao B, Qian H, Bi G, Song S, Yang J J and Wu H 2019 *Adv. Mater.* **31** 1902761
[5] Chua L 1971 *IEEE Trans. Circuit Theory* **18** 507
[6] Strukov D B, Snider G S, Stewart D R and Williams R S 2008 *Nature* **453** 80
[7] Zhao X, Xu H, Wang Z, Lin Y and Liu Y 2019 *InfoMat* **1** 183
[8] Jo S H, Chang T, Ebong I, Bhadviya B B, Mazumder P and Lu W 2010 *Nano Lett.* **10** 1297
[9] Wang Z Q, Xu H Y, Li X H, Yu H, Liu Y C and Zhu X J 2012 *Adv. Func. Mater.* **22** 2759
[10] Yang Y C, Pan F, Liu Q, Liu M and Zeng F 2009 *Nano Lett.* **9** 1636
[11] Chen J Y, Hsin C L, Huang C W, Chiu C H, Huang Y T, Lin S J, Wu W W and Chen L J 2013 *Nano Lett.* **13** 3671
[12] Yang J J, Borghetti J, Murphy D, Stewart D R and Williams R S 2009 *Adv. Mater.* **21** 3754
[13] Yao P, Wu H, Gao B, Eryilmaz S B, Huang X, Zhang W, Zhang Q, Deng N, Shi L, Wong H P and Qian H 2017 *Nat. Commun.* **8** 15199
[14] Gao S, Liu G, Yang H, Hu C, Chen Q, Gong G, Xue W, Yi X, Shang J and Li R W 2019 *ACS Nano* **13** 2634
[15] Chen S, Lou Z, Chen D and Shen G 2018 *Adv. Mater.* **30** 1705400
[16] Lee G J, Choi C, Kim D H and Song Y M 2017 *Adv. Funct. Mater.* **28** 1705202
[17] Tan H, Liu G, Zhu X, Yang H, Chen B, Chen X, Shang J, Lu W D, Wu Y and Li R W 2015 *Adv. Mater.* **27** 2797
[18] Tan H, Liu G, Yang H, Yi X, Pan L, Shang J, Long S, Liu M, Wu Y and Li R W 2017 *ACS Nano* **11** 11298
[19] Chen G, Song C, Chen C, Gao S, Zeng F and Pan F 2012 *Adv. Mater.* **24** 3515
[20] Yang J J, Pickett M D, Li X, Ohlberg D A, Stewart D R and Williams R S 2008 *Nat. Nanotechnol.* **3** 429
[21] You T, Du N, Slesazeck S, Mikolajick T, Li G, Burger D, Skorupa I, Stocker H, Abendroth B, Beyer A, Volz K, Schmidt O G and Schmidt H 2014 *ACS Appl. Mater. Interfaces* **6** 19758
[22] Davis C B, Allred D D, Reyes-Mena A, González-Hernández J, González O, Hess B C and Allred W P 1993 *Phys. Rev. B* **47** 13363
[23] Dang X Z, Wang C D, Yu E T, Boutros K S and Redwing J M 1998 *Appl. Phys. Lett.* **72** 2745
[24] Skorodumova N V, Simak S I, Lundqvist B I, Abrikosov I A and Johansson B 2002 *Phys. Rev. Lett.* **89** 166601
[25] Nesheva D, Levi Z, Aneva Z, Nikolova V and Hofmeister H 2000 *J. Phys.: Condens. Matter.* **12** 751
[26] Zhou F, Zhou Z, Chen J, Choy T H, Wang J, Zhang N, Lin Z, Yu S, Kang J, Wong H P and Chai Y 2019 *Nat. Nanotechnol.* **14** 776
[27] Cai S Y, Tzou C Y, Liou Y R, Chen D R, Jiang C Y, Ma J M, Chang C Y, Tseng C Y, Liao Y M, Hsieh Y P, Hofmann M and Chen Y F 2019 *ACS Appl. Mater. Interfaces* **11** 4649
[28] Yang C S, Shang D S, Liu N, Fuller E J, Agrawal S, Talin A A, Li Y Q, Shen B G and Sun Y 2018 *Adv. Funct. Mater.* **28** 1804170
[29] Karbalaei Akbari M and Zhuiykov S 2019 *Nat. Commun.* **10** 3873
[30] Zhao X, Wang Z, Xie Y, Xu H, Zhu J, Zhang X, Liu W, Yang G, Ma J and Liu Y 2018 *Small* **14** 1801325
[31] Kumar M, Kim H S and Kim J 2019 *Adv. Mater.* **31** 1900021
[32] Ren Y, Hu L, Mao J Y, Yuan J, Zeng Y J, Ruan S, Yang J Q, Zhou L, Zhou Y and Han S T 2018 *J. Mater. Chem. C* **6** 9383
[33] Alquraishi W, Fu Y, Qiu W, Wang J, Chen Y, Kong L A, Sun J and Gao Y 2019 *Org. Electron.* **71** 72
[34] Fan L, Chen Y, Liu Q, Chen S, Zhu L, Meng Q, Wang B, Zhang Q, Ren H and Zou C 2016 *ACS Appl. Mater. Interfaces* **8** 32971
[35] Wu Q, Wang J, Cao J, Lu C, Yang G, Shi X, Chuai X, Gong Y, Su Y, Zhao Y, Lu N, Geng D, Wang H, Li L and Liu M 2018 *Adv. Electron. Mater.* **4** 1800556
[36] Li H K, Chen T P, Liu P, Hu S G, Liu Y, Zhang Q and Lee P S 2016 *J. Appl. Phys.* **119** 244505
[37] Wu Y, Wei Y, Huang Y, Cao F, Yu D, Li X and Zeng H 2017 *Nano Res.* **10** 1584
[38] Chen Y, Liu G, Wang C, Zhang W, Li R W and Wang L 2014 *Mater. Horiz.* **1** 489
[39] Liu G, Wang C, Zhang W, Pan L, Zhang C, Yang X, Fan F, Chen Y and Li R W 2016 *Adv. Electron. Mater.* **2** 1500298
[40] Fang L, Dai S, Zhao Y, Liu D and Huang J 2019 *Adv. Electron. Mater.* 1901217
[41] Nau S, Wolf C, Sax S and List-Kratochvil E J 2015 *Adv. Mater.* **27** 1048
[42] Zhang L, Pasthukova N, Yao Y, Zhong X, Pavlica E, Bratina G, Orgiu E and Samori P 2018 *Adv. Mater.* **30** 1801181
[43] Jaafar A H, Gray R J, Verrelli E, O'Neill M, Kelly S M and Kemp N T 2017 *Nanoscale* **9** 17091
[44] Sun Y, Tai M, Song C, Wang Z, Yin J, Li F, Wu H, Zeng F, Lin H and Pan F 2018 *J. Phys. Chem. C* **122** 6431
[45] Choi J, Le Q V, Hong K, Moon C W, Han J S, Kwon K C, Cha P R, Kwon Y, Kim S Y and Jang H W 2017 *ACS Appl. Mater. Interfaces* **9** 30764
[46] Gu C and Lee J S 2016 *ACS Nano* **10** 5413
[47] Kim Y C, Kim K H, Son D Y, Jeong D N, Seo J Y, Choi Y S, Han I T, Lee S Y and Park N G 2017 *Nature* **550** 87
[48] Kim D J, Tak Y J, Kim W G, Kim J K, Kim J H and Kim H J 2017 *Adv. Mater. Interfaces* **4** 1601035
[49] Zhu X, Lee J and Lu W D 2017 *Adv. Mater.* **29** 1700527
[50] Zhu X and Lu W D 2018 *ACS Nano* **12** 1242
[51] Ham S, Choi S, Cho H, Na S I and Wang G 2019 *Adv. Funct. Mater.* **29** 1806646
[52] Zhou F, Liu Y, Shen X, Wang M, Yuan F and Chai Y 2018 *Adv. Funct. Mater.* **28** 1800080
[53] Anichini C, Czepa W, Pakulski D, Aliprandi A, Ciesielski A and Samorì P 2018 *Chem. Soc. Rev.* **47** 4860
[54] He Q, Wu S, Yin Z and Zhang H 2012 *Chem. Sci.* **3** 1764
[55] Wu S, He Q, Tan C, Wang Y and Zhang H 2013 *Small* **9** 1160
[56] Liu M, Yin X, Ulin-Avila E, Geng B, Zentgraf T, Ju L, Wang F and Zhang X 2011 *Nature* **474** 64
[57] Qiao H, Yuan J, Xu Z, Chen C, Lin S, Wang Y, Song J, Liu Y, Khan Q, Hoh H Y, Pan C X, Li S and Bao Q 2015 *ACS Nano* **9** 1886
[58] Yan F, Wei Z, Wei X, Lv Q, Zhu W and Wang K 2018 *Small Methods* **2** 1700349
[59] Huo N and Konstantatos G 2018 *Adv. Mater.* **30** 1801164
[60] Liu C, Yan X, Song X, Ding S, Zhang D W and Zhou P 2018 *Nat. Nanotech.* **13** 404
[61] Wu X, Ge R, Chen P A, Chou H, Zhang Z, Zhang Y, Banerjee S, Chiang M H, Lee J C and Akinwande D 2019 *Adv. Mater.* **31** 1806790
[62] Wang M, Cai S, Pan C, Wang C, Lian X, Zhuo Y, Xu K, Cao T, Pan X, Wang B, Liang S J, Yang J J, Wang P and Miao F 2018 *Nat. Electron.* **1** 130
[63] Seo S, Jo S H, Kim S, Shim J, Oh S, Kim J H, Heo K, Choi J W, Choi C, Oh S, Kuzum D, Wong H P and Park J H 2018 *Nat. Commun.* **9** 5106
[64] Ni Z, Wang Y, Liu L, Zhao S, Xu Y, Pi X and Yang D 2018 *IEDM 2018 IEEE Int.* 18-887
[65] Wang W, Panin G N, Fu X, Zhang L, Ilanchezhiyan P, Pelenovich V O, Fu D and Kang T W 2016 *Sci. Rep.* **6** 31224
[66] Campbell K A, Bassine R A, Kabir M F and Astle J 2018 *ACS Appl. Electron. Mater.* **1** 96
[67] Lipatov A, Sharma P, Gruverman A and Sinitskii A 2015 *ACS Nano* **9** 8089
[68] He H K, Yang R, Zhou W, Huang H M, Xiong J, Gan L, Zhai T Y and Guo X 2018 *Small* **14** 1800079
[69] Tran M D, Kim H, Kim J S, Doan M H, Chau T K, Vu Q A, Kim J H and Lee Y H 2019 *Adv. Mater.* **31** 1807075
[70] Lee J, Pak S, Lee Y W, Cho Y, Hong J, Giraud P, Shin H S, Morris S M, Sohn J I, Cha S and Kim J M 2017 *Nat. Commun.* **8** 14734
[71] Lee D, Hwang E, Lee Y, Choi Y, Kim J S, Lee S and Cho J H 2016 *Adv. Mater.* **28** 9196
[72] Qin S Wang F, Liu Y, Wan Q, Wang X, Xu Y, Shi Y and Wang X 2017 *2D Mater.* **4** 035022
[73] Xiang D, Liu T, Xu J, Tan J Y, Hu Z, Lei B, Zheng Y, Wu J, Neto A H C, Liu L and Chen W 2018 *Nat. Commun.* **9** 2966

[74] Maier P, Hartmann F, Emmerling M, Schneider C, Kamp M, Höfling S and Worschech L 2016 *Phys. Rev. Appl.* **5** 054011

[75] Maier P, Hartmann F, Rebello Sousa Dias M, Emmerling M, Schneider C, Castelano L K, Kamp M, Marques G E, Lopez-Richard V, Worschech L and Höfling S 2016 *Appl. Phys. Lett.* **109** 023501

[76] Wang Y, Lv Z, Liao Q, Shan H, Chen J, Zhou Y, Zhou L, Chen X, Roy V A L, Wang Z, Xu Z, Zeng Y J and Han S T 2018 *Adv. Mater.* **30** 1800327

[77] Yang Y C, Pan F, Liu Q, Liu M and Zeng F 2009 *Nano Lett.* **9** 1636

[78] Jeong D S, Schroeder H and Waser R 2009 *Phys. Rev. B* **79** 195317

[79] Kalsbeck W A and Holden Thorp H 1991 *J. Efectroanal. Chem.* **314** 363

[80] Kumar M, Abbas S and Kim J 2018 *ACS Appl. Mater. Interfaces* **10** 34370

[81] Zhai Y, Yang X, Wang F, Li Z, Ding G, Qiu Z, Wang Y, Zhou Y and Han S T 2018 *Adv. Mater.* **30** 1803563

[82] Bandara H M and Burdette S C 2012 *Chem. Soc. Rev.* **41** 1809

[83] Tanaka K and Shimakawa K 2011 *Amorphous Chalcogenide Semiconductors and Related Materials* (New York: Springer) p. 185

[84] Yager K G, Tanchak O M, Godbout C, Fritzsche H and Barrett C J 2006 *Macromolecules* **39** 9311

[85] Ling H, Tan K, Fang Q, Xu X, Chen H, Li W, Liu Y, Wang L, Yi M, Huang R Qian Y, Xie L and Huang W 2017 *Adv. Electron. Mater.* **3** 1600416

[86] Qiu H, Zhao Y, Liu Z, Herder M, Hecht S and Samori P 2019 *Adv. Mater.* **31** 1903402

[87] deQuilettes D W, Zhang W, Burlakov V M, Graham D J, Leijtens T, Osherov A, Bulovic V, Snaith H J, Ginger D S and Stranks S D 2016 *Nat. Commun.* **7** 11683

[88] Wang Y, Yang J, Wang Z, Chen J, Yang Q, Lv Z, Zhou Y, Zhai Y, Li Z and Han S T 2019 *Small* **15** 1805431

[89] Zhou Y, Yew K S, Ang D S, Kawashima T, Bera M K, Zhang H Z and Bersuker G 2015 *Appl. Phys. Lett.* **107** 072107

[90] Kawashima T, Zhou Y, Yew K S and Ang D S 2017 *Appl. Phys. Lett.* **111** 113505

[91] Emboras A, Niegemann J, Ma P, Haffner C, Pedersen A, Luisier M, Hafner C, Schimmel T and Leuthold J 2016 *Nano Lett.* **16** 709

[92] Emboras A, Goykhman I, Desiatov B, Mazurski N, Stern L, Shappir J and Levy U 2013 *Nano Lett.* **13** 6151

[93] Yao J N, Loo B H, Hashimoto K and Fujishima A 1990 *J. Electroanal. Chem.* **290** 263

[94] Wang S, Fan W, Liu Z, Yu A and Jiang X 2018 *J. Mater. Chem. C* **6** 191

[95] Liu Q, Sun J, Lv H, Long S, Yin K, Wan N, Li Y, Sun L and Liu M 2012 *Adv. Mater.* **24** 1844

[96] Tsuruoka T, Valov I, Tappertzhofen S, van den Hurk J, Hasegawa T, Waser R and Aono M 2015 *Adv. Funct. Mater.* **25** 6374

[97] Xiao Z and Huang J 2016 *Adv. Electron. Mater.* **2** 1600100

[98] Yizhar O, Fenno L E, Davidson T J, Mogri M and Deisseroth K 2011 *Neuron* **71** 9

[99] Wang Y, Yang J, Ye W, She D, Chen J, Lv Z, Roy V A L, Li H, Zhou K, Yang Q, Zhou Y and Han S T 2019 *Adv. Electron. Mater.* 1900765

[100] Shao L, Wang H, Yang Y, He Y, Tang Y, Fang H, Zhao J, Xiao H, Liang K, Wei M, Xu W, Luo M, Wan Q, Hu W, Gao T and Cui Z 2019 *ACS Appl. Mater. Interfaces* **11** 12161

[101] Wang G, Wang R, Kong W and Zhang J 2018 *Analysis. Cogn. Neurodyn.* **12** 615

[102] Zhou F, Chen J, Tao X, Wang, X and Chai Y 2019 *Research* **2019**